PERISTALTIC PUMPING OF AN ELLIS FLUID IN AN INCLINED ASYMMETRIC CHANNEL

A. SMALL, P. NAGARANI*, M. NARAHARI

ABSTRACT. The flow of an incompressible Ellis fluid in an inclined asymmetric channel, driven by peristaltic waves was studied under low Reynolds number and long wavelength assumptions. The wave on each side of the channel are assumed to be an infinite train of sinusoidal waves, both having the same constant wave speed and wavelength however, they vary in wave amplitude, channel half width and phase angle. We derived expressions for the axial and transverse velocities, volume flow rate, pressure rise per unit wavelength and streamlines. The effects of varying the wave amplitudes, the phase angle, the channel width, the angle of inclination of the channel as well as the fluid parameters on the flow were analyzed. Trapping conditions were determined and the presence of reflux highlighted using the streamlines for the necessary channel and fluid conditions. By varying the fluid parameters, changes in the fluid that deviated from the Newtonian case resulted in a reduction in the axial velocity in the neighborhood of the center of the channel and a simultaneous increase in the velocity at the periphery of the channel. A nonlinear relation was observed with the pressure rise and the volume flow rate. This nonlinear relation is more pronounced with an increase in the absolute value of the volume flow rate. For Newtonian fluids a linear relation exists between these two variables. The fluid parameters had little effects on the streamlines. However, variations of the wave amplitudes, volume flow, channel width and phase angle had greater effects on the streamlines and hence the trapped region.

AMS Mathematics Subject Classification : 76A05, 76Dxx, 92C10.
Key words and phrases : Non-Newtonian fluids, shear-thinning fluids, Lubrication Theory, Peristalsis.

1. Introduction

Peristalsis is the transport of fluids in conduits due to transverse systematic wavelike displacements of the walls of the conduits. The waves propagate in the

axial or longitudinal direction along the length of the conduit. This method of pumping is preferred to other pumping processes when it is necessary to preserve the integrity of the fluids. For example, when transporting acidic and corrosive fluids, this means of transport is suitable, as the fluid is never in contact with the mechanical parts of the pump. Peristalsis is the primary means of transport in human physiological fluid transport, as well as fluid transport in other organisms. The transport of chime within the esophagus, ovum within the oviducts, urine within the ureter, and blood flow within small veins is accomplished using peristalsis. Some worms use this means of fluid movement to achieve locomotion.

Latham [10], made early mathematical contributions to the understanding of peristalsis. However, this pumping process was well observed in varying physiologies decades earlier [21]. Fung and Yih [5] also made attempts to understand this method of transport by including the non-linear convective accelerations under small wave amplitudes within a channel. They found that the mean flow induced by the wall is proportional to the square of the wave amplitude. The velocity of the fluid was observed to be dependent on the mean pressure gradient and for a particular critical pressure gradient, the velocity was zero. There was no reflux for pressure gradients less than this critical pressure gradient. However, for values of the pressure gradient exceeding this critical value, a backward flow is induced. Later, the infinite long tube model was investigated by Shapiro *et al.* [21] for Newtonian fluids under the assumption of long wavelength and low Reynolds number. This model was analysed for both channels and tubes and the reflux and trapping phenomena were explored. The pumping performance was determined by considering the relation between the pressure rise per unit wavelength and the time-averaged volume flow rate and it was shown that the relationship between these two quantities was linear. Manton [11] investigated the long-wavelength peristaltic pumping at low Reynolds number for long peristaltic waves of arbitrary shapes and obtained asymptotic solutions for the wave fields. Manton also confirmed the conditions for trapping to occur considering arbitrary wave shapes and established that reflux occurs whenever there is an adverse mean pressure gradient. Non-linear peristaltic transport in an inclined asymmetric channel through a porous medium was investigated by Kothandapani and Srinivas [8]. Srinivas and Gayathri [23] considered the peristaltic transport of a Newtonian fluid in a vertical asymmetric channel with heat transfer and porouos medium. The effects of permeability, sources and sinks of heat, phase difference of the waves along the channel, channel width and wave amplitude on the velocity, pressure gradient, shear stress and trapping phenomenon were investigated.

The study of non-Newtonian fluid flows has gained a lot of attention from researchers, due to its applications in chemical processing industries, polymer processing industries and biomedical flows. In order to gain knowledge of these processes, several researchers have been working with different non-Newtonian fluid models by considering varying geometries, wave shapes, and flow conditions. Srivastava and Srivastava [22] considered the peristaltic transport of a

non-Newtonian fluid for application to the Vas Deferens and small intestine. The model was studied with the assumptions of long wavelength and zero Reynolds number, with the fluid modelled by a power-law fluid. The results obtained were compared with results for the Newtonian models as well as with experimental information obtained from observations made in the Vas Deferens and small intestine. Peristaltic transport of two-layered power-law fluid within axisymmetric tubes was studied by Usha and Rao [25]. This fluid type was chosen for the periphery and core independently and could exhibit either Newtonian shear thinning or shear thickening behavior in both regions. It was observed that the rheology of the outer layer fluid is the key factor in the mean flow being either positive or negative. Mernone *et al.* [12] considered peristaltic transport of a Casson fluid within channels. Here a perturbation series solution of the stream function was used with the perturbation parameter being the amplitude ratio. Numerical and analytical solutions of the stream function were obtained. It was realized that the Casson model can be considered as an extension of the Newtonian model which may be sufficient to describe some physiological flows. The effects of a third-order fluid on peristaltic transport was studied by Hayat *et al.* [6] within circular cylindrical tubes. Here also, both analytical (perturbation) and numerical solutions were provided. Comparisons of the analytic and numeric solutions were made. Naga Rani and Sarojamma [15] studied the peristaltic transport of a Casson fluid in an asymmetric channel. The asymmetry of the walls was achieved by considering the waves along the walls of the channel with different amplitudes, and phase differences. Rao and Mishra [19] investigated the peristaltic transport of a power-law fluid in a porous tube. Vajravelu *et al.* [26] analyzed the flow of a Herschel-Bulkley fluid in a channel due to peristaltic pumping and the effects of yield stress and wave amplitude were investigated. The trapping phenomenon was also discussed for Newtonian, power-law, and Herschel-Bulkley fluids. Later, they investigated the peristaltic transport of a Herschel-Bulkley fluid in an inclined tube [27]. The results for Bingham, Newtonian and power-law fluids were produced. The effects of the fluid parameters on the flow were also analyzed. Hariharan *et al.* [9] considered the peristaltic transport of non-Newtonian fluids in diverging tubes. Here the flowing fluid was modelled by power-law and Bingham constitutive relations and several wave types were considered. For each constitutive relation, the time average pressure rise and the flow rate relationship were examined for different fluid parameters. It was established that reflux strongly depends on the wave shape and fluid parameter. The peristaltic flow of a Casson fluid within the annular gap between two coaxial tubes was investigated by Nagarani and Lewis [16]. In this study, the inner tube is rigid and the peristaltic wave propagates along the outer tube. The effects of yield stress and annular gap on the transport process were analysed. It was found that yield stress and annular gap have significant influence on the pressure rise, frictional force at the walls and the trapping phenomenon. Abbasi, *et al.* [1] studied the flow Carreau-Yasuda fluid

in an asymmetric channel due to peristalsis. They obtained solutions to the governing equations numerically. Eldabe *et al.* [3] also investigated the peristaltic motion of a nano non-Newtonian fluid which obeys Carreau model through a porous medium inside an asymmetric channel and similarly produced numerical solutions to the governing equations. They also observed heat and mass flow. Recently, Noreen*et al.* [18] studied the heat transfer characteristics on peristalsis in an inclined asymmetric channel using Carreau fluid model. This study revealed that the temperature characteristics depend significantly on the inclination of the magnetic field. Saleem *et al.* [20], investigated the electro-osmotic peristaltic flow in a Casson fluid and studied the Joule heating and viscous effects using the lubrication approach. Gendy *et al.* [4], constructed a 3D simulation of a peristaltic micro-pump by considering the Carreau and power-law fluid models using ANSYS Fluent in application to biomedical engineering. Peristaltic transport in a duct with an elliptic cross-section of a Jeffrey fluid was analyzed by Nadeem *et al.* [14] while analyzing the viscous effects on heat transfer.

Very few papers are available in the literature on Ellis fluid flows till date. The flow of an Ellis fluid in a slit was studied by Steller [24]. Here both planar and annular slits were discussed and compared. It was concluded that the planar and annular slit flows are qualitatively similar, however, the quantitative differences between the two cases are more pronounced for strongly non-Newtonian fluids. Gravity driven thin film flow of an Ellis fluid, was studied by Kheyfets and Kieweg [7]. They developed 3D numerical solution and the particular cases of results were verified experimentally. Peristaltic pumping of Ellis fluid in channel was studied by Ali *et al.* [2] under long wavelength and low Reynolds number assumption. The response of the fluid flow to changes in the fluid parameters was investigated. It was observed that for a fixed volume flow rate the pressure rise per unit wavelength increases with increase in the fluid parameter α.

This paper investigates the flow of an Ellis fluid in a channel that is inclined with some angle. The waves travelling along the channel walls are asymmetric in nature. The asymmetry is established by considering the waves of the same speed and wavelength travelling along the walls with different mean mid width, amplitude and phase angle. The widely used assumptions of low Reynolds number, long wavelength are used to study the model. The mathematical formulation of the model and assumptions made in establishing the model are outlined in section 2 and the method of solution is presented in section 3. We have discussed the results with the aid of plots of axial velocity, velocity vector field, streamlines as well as the pressure rise per unit wavelength in section 4 and the concluding remarks of the study were given in section 5.

2. Mathematical Formulation

We consider the flow of a non-Newtonian fluid (Ellis fluid) in an infinitely long, inclined, asymmetric channel, being driven by sinusoidal peristaltic waves as shown in Fig. 1. The Ellis fluid model captures a wide range of yield free fluids,
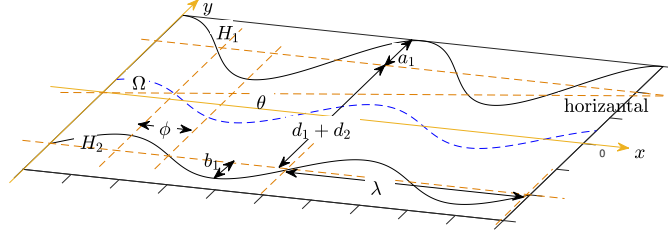
FIGURE 1. Peristaltic wave propagating along assymetric channel wall

for this reason, this model is chosen to exploit the advantages of considering these non-Newtonian fluid. For this model, the shear stress as a function of the deformation is given by equation (1) [17].

$$\tau_{ij} = \left(\frac{\mu_0}{1 + \left| \frac{II_\tau}{2\tau_0^2} \right|^{\frac{\alpha-1}{2}}} \right) \gamma_{ij}. \tag{1}$$

Here τ_{ij} and γ_{ij} are the stress and deformation tensors respectively, μ_0 is the zero stress or Newtonian viscosity, $(\alpha > 1)$ is a curve fitting constant related with the particular fluid and is a measure of the extent of shear thinning, τ_0 is the shear stress at which the viscosity of the fluid is half the zero stress viscosity and II_τ is the second invariant of the stress tensor. The cases $\tau_0 \to \infty$ and $\left| (II_\tau)/(2\tau_0^2) \right|^{(\alpha-1)/2} >> 1$ reduces the relation to the Newtonian and power-law constitutive relations respectively. Since the Ellis fluid model can be reduced to the power-law model at high shear stress. Therefore, for this condition some power-law fluids that can be modelled as Ellis fluids are human blood, tomato ketchup, yoghurt, peanut butter, mayonnaise, nylon, toothpaste mascara, nail polish and oil of Olay naming a few [17].

The governing equations of the problem are the conservation of mass and momentum equations in Cartesian coordinates system, which in compact vector forms are given as:

$$\frac{\partial \rho}{\partial t} + \nabla . \rho \mathbf{U} = 0, \tag{2}$$

$$\frac{D\mathbf{U}}{Dt} = -\frac{1}{\rho}\nabla p + \frac{1}{\rho}\nabla . \tau + \mathbf{g}. \tag{3}$$

Here $\mathbf{U} = \langle u, v, w \rangle$ is the velocity vector, p is the pressure,

$$\tau = \left\{ \begin{array}{ccc} \tau_{xx} & \tau_{xy} & \tau_{xz} \\ \tau_{yx} & \tau_{yy} & \tau_{yz} \\ \tau_{zx} & \tau_{zy} & \tau_{zz} \end{array} \right\},$$

is the shear stress tensor and $\mathbf{g} = \langle g_x, g_y, g_z \rangle$ the acceleration due to gravity. The assumptions that the flow is only in the x and y directions, that is the flow does not vary in the z direction, the channel is inclined at an angle θ and that the flow is incompressible, reduces these equations to:

$$\frac{\partial u}{\partial x} + \frac{\partial v}{\partial y} = 0, \tag{4}$$

$$\frac{\partial u}{\partial t} + u\frac{\partial u}{\partial x} + v\frac{\partial u}{\partial y} = -\frac{1}{\rho}\left\{\frac{\partial p}{\partial x} + \frac{\partial \tau_{xx}}{\partial x} + \frac{\partial \tau_{xy}}{\partial y}\right\} + g\sin\theta, \tag{5}$$

$$\frac{\partial v}{\partial t} + u\frac{\partial v}{\partial x} + v\frac{\partial v}{\partial y} = -\frac{1}{\rho}\left\{\frac{\partial p}{\partial y} + \frac{\partial \tau_{yx}}{\partial x} + \frac{\partial \tau_{yy}}{\partial y}\right\} - g\cos\theta. \tag{6}$$

These equations are subjected to the following boundary conditions:

$$\tau_{x,y}\Big|_{y=\Omega} = \psi\Big|_{y=\Omega} = \frac{\partial u}{\partial y}\Big|_{y=\Omega} = 0, \quad u\Big|_{y=H_1} = u\Big|_{y=H_2} = 0, \quad v\Big|_{y=\Omega} = 0, \tag{7}$$

where $\Omega = \frac{H_1 + H_2}{2}$. The wall shapes for the upper and lower walls are assumed respectively as,

$$H_1(x,t) = d_1 + a_1\cos\left\{\frac{2\pi(x-ct)}{\lambda}\right\}, \tag{8}$$

$$H_2(x,t) = -d_2 - b_1\cos\left\{\frac{2\pi(x-ct)}{\lambda} + \phi\right\}. \tag{9}$$

Here $d_1 + d_2$ is the width of the channel, a_1 and b_1 are the amplitudes of the upper and lower peristaltic waves respectively, c is the speed of the wave, λ the wavelength and $\phi \in [0, \pi]$ is the phase angle. When $d_1 = d_2, a_1 = b_1$ and $\phi = 0$, equations (8) and (9) correspond to the symmetric channel case and further $a_1^2 + b_1^2 + 2a_1 b_1 \cos\phi \leq (d_1 + d_2)^2$. We observed the flow from the wave frame of reference with coordinates $(\hat{x}, \hat{y})$ by using the Galilean transformation,

$$x = \hat{x} + ct, \quad y = \hat{y}, \quad t = \hat{t}, \quad u = \hat{u} + c, \quad v = \hat{v}, \quad p = \hat{p}, \quad \tau_{x,y} = \hat{\tau}_{\hat{x}\hat{y}}. \tag{10}$$

We also introduce the dimensionless quantities,

$$x^* = \frac{\hat{x}}{\lambda}, \quad y^* = \frac{\hat{y}}{d_1}, \quad t^* = \frac{c\hat{t}}{\lambda}, \quad u^* = \frac{\hat{u}}{c}, \quad v^* = \frac{\hat{v}}{c\delta}, \quad \delta = \frac{d_1}{\lambda}, \quad h_1 = \frac{\hat{H}_1}{d_1},$$

$$h_2 = \frac{\hat{H}_2}{d_1}, \quad a = \frac{a_1}{d_1}, \quad d = \frac{d_2}{d_1}, \quad b = \frac{b_1}{d_1} \quad \tau^*_{x^* x^*} = \frac{\lambda\hat{\tau}_{\hat{x}\hat{x}}}{\mu_0 c}, \quad \tau^*_{y^* x^*} = \frac{d_1\hat{\tau}_{\hat{y}\hat{x}}}{\mu_0 c},$$

$$\tau^*_{y^* y^*} = \frac{d_1\hat{\tau}_{\hat{y}\hat{y}}}{\mu_0 c}, \quad \tau^*_0 = \frac{d_1\hat{\tau}_0}{\mu_0 c}, \quad \psi^* = \frac{a\psi}{c}, \quad p^* = \frac{\hat{p}d_1\delta}{\mu_0 c}, q^* = \frac{\hat{q}}{d_1 c}, \quad Q^* = \frac{\hat{Q}}{d_1 c},$$

$$Re = \frac{\rho d_1 c}{\mu_0}, \quad F = \frac{\mu_0 c}{\rho g d_1^2} \quad \Lambda = \frac{h_1 + h_2}{2}. \tag{11}$$

By substituting the above non-dimensional quantities, the equations (4) – (6), can be written as

$$\frac{\partial u^*}{\partial x^*} + \frac{\partial v^*}{\partial y^*} = 0, \tag{12}$$

$$\delta Re\left(u^*\frac{\partial u^*}{\partial x^*} + v^*\frac{\partial u^*}{\partial y^*}\right) = -\frac{\partial p^*}{\partial x^*} - \delta^2\frac{\partial \tau^*_{x^*x^*}}{\partial x^*} - \frac{\partial \tau^*_{x^*y^*}}{\partial y^*} + \frac{\sin\theta}{F}, \qquad (13)$$

$$\delta^3 Re\left(u^*\frac{\partial v^*}{\partial x^*} + v^*\frac{\partial v^*}{\partial y^*}\right) = -\frac{\partial p^*}{\partial y^*} - \delta^2\frac{\partial \tau^*_{x^*x^*}}{\partial x^*} - \delta\frac{\partial \tau^*_{y^*y^*}}{\partial y^*} - \delta\frac{\cos\theta}{F}. \qquad (14)$$

By neglecting the terms of order δ and above, from (13) and (14), we have

$$-\frac{\partial p^*}{\partial x^*} - \frac{\partial \tau^*_{y^*x^*}}{\partial y^*} + \frac{\sin\theta}{F} = 0, \qquad (15)$$

$$\frac{\partial p^*}{\partial y^*} = 0. \qquad (16)$$

The non-dimensional wall equations are given by the expressions

$$h_1(x^*) = 1 + a\cos(2\pi x^*), \qquad (17)$$
$$h_2(x^*) = -d - b\cos(2\pi x^* + \phi). \qquad (18)$$

Here we have $a^2 + b^2 + 2ab\cos\phi \le (1+d)^2$. The constitutive relation for the single stress component remaining is

$$\tau^*_{y^*x^*} = \frac{1}{\left[1 + \left|\frac{\tau^*_{x^*y^*}}{\tau^*_0}\right|^{\alpha-1}\right]}\left(-\frac{\partial u^*}{\partial y^*}\right). \qquad (19)$$

The corresponding boundary conditions in non-dimensional form are obtained as:

$$\tau^*_{y^*x^*}\big|_{y^*=\Lambda} = \psi^*\big|_{y^*=\Lambda} = \frac{\partial u^*}{\partial y^*}\big|_{y^*=\Lambda} = 0, \quad u^*\big|_{y^*=h_1} = u^*\big|_{y^*=h_2} - 1, \quad v^*\big|_{y^*=\Lambda} = 0. \qquad (20)$$

3. Method of Solution

Rewriting equations (15) and (16) without stars we solve, using (17) and (19) and the conditions given in (20), for τ_{xy} which gives

$$\tau_{xy} = M\left(y - \Lambda\right) \qquad (21)$$

where $P = -dp/dx$, $M = P + f$ and $f = (\sin\theta)/F$. Substituting equation (21) into equation (19) and using the conditions (20) we obtain the axial velocity as

$$u(x,y) = M\left[\frac{1}{2}\left(h_1^2 - y^2\right) - \Lambda\left(h_1 - y\right) + \left|\frac{M}{\tau_0}\right|^{\alpha-1}\frac{1}{\alpha+1}\left(\left(h_1-\Lambda\right)^{\alpha+1} - \left|y-\Lambda\right|^{\alpha+1}\right)\right] - 1, \qquad (22)$$

From (12), we obtained the transverse velocity as

$$v(x,y) = M'\left[\frac{1}{6}\left(y^3 - \Lambda^3\right) - \frac{\Lambda}{2}\left(y^2 - \Lambda^2\right) + \left(\Lambda - \frac{h_1}{2}\right)h_1\left(y - \Lambda\right)\right.$$

$$-\frac{\alpha}{\alpha+1}\left|\frac{M}{\tau_0}\right|^{\alpha-1}\left(\left(h_1-\Lambda\right)^{\alpha+1}\left(y-\Lambda\right)-\frac{\left|y-\Lambda\right|^{\alpha+2}}{\alpha+2}sign\left(y-\Lambda\right)\right)\Bigg]+$$

$$M\Bigg[-\frac{\Lambda'}{2}\left(y^2-\Lambda^2\right)+\left(\Lambda'h_1+\Lambda h_1'-h_1h_1'\right)\left(y-\Lambda\right)$$

$$-\left|\frac{M}{\tau_0}\right|^{\alpha-1}\left(\left(h_1-\Lambda\right)^{\alpha}\left(h_1'-\Lambda'\right)\left(y-\Lambda\right)+\frac{\left|y-\Lambda\right|^{\alpha+1}}{\alpha+1}\Lambda'\right)\Bigg]. \tag{23}$$

The stream function ψ is obtained as

$$\psi(x,y)=M\Bigg[-\frac{1}{6}\left(y-h_1\right)^2\left(y-2h_1\right)+\frac{\Lambda}{2}\left(y-h_1\right)^2+$$

$$\left|\frac{M}{\tau_0}\right|^{\alpha-1}\frac{1}{\alpha+1}\left(\left(h_1-\Lambda\right)^{\alpha+1}\left(y-h_1\right)-\frac{\left|y-\Lambda\right|^{\alpha+2}}{\alpha+2}sign(y-\Lambda)\right.$$

$$\left.+\frac{\left(h_1-\Lambda\right)^{\alpha+2}}{\alpha+2}\right)\Bigg]-\left(y-h_1\right)+\frac{q}{2}. \tag{24}$$

Now the volume flow rate is given by

$$q(x)=\int_{h_2}^{h_1}u\,dy, \tag{25}$$

which gives,

$$q(x) \;=\; M\Bigg[\frac{2}{3}\left(h_1-\Lambda\right)^2\left(2h_1+h_2\right)-2\Lambda\left(h_1-\Lambda\right)^2+\frac{2}{\alpha+2}\left|\frac{M}{\tau_0}\right|^{\alpha-1}\left(h_1-\Lambda\right)^{\alpha+2}\Bigg]$$

$$-\;2\left(h_1-\Lambda\right). \tag{26}$$

3.1. Symmetric Case. In the case of a symmetric channel i.e. when $d=1, a=b$ and $\phi=0$, we have $h_2=-h_1=h$ and $\Lambda=0$, the expressions for axial and transverse velocities are obtained as

$$u(x,y)=M\left[\frac{1}{2}\left(h^2-y^2\right)+\frac{1}{\alpha+1}\left|\frac{M}{\tau_0}\right|^{\alpha-1}\left(h^{\alpha+1}-y^{\alpha+1}\right)\right]-1 \tag{27}$$

$$v(x,y)=-M'\left[\frac{1}{2}\left(h^2y-\frac{y^3}{3}\right)+\frac{\alpha}{\alpha+1}\left|\frac{M}{\tau_0}\right|^{\alpha-1}\left(h^{\alpha+1}y-\frac{y^{\alpha+2}}{\alpha+2}\right)\right]$$

$$-M\left[hh'y+\left|\frac{M}{\tau_0}\right|^{\alpha-1}h'h^{\alpha}y\right] \tag{28}$$

The stream function ψ is reduced to,

$$\psi(x,y)=\frac{M}{2}\left[\left(h^2y-\frac{y^3}{3}\right)+\frac{2}{\alpha+1}\left|\frac{M}{\tau_0}\right|^{\alpha-1}\left(h^{\alpha+1}y-\frac{y^{\alpha+2}}{\alpha+2}\right)\right]-y \tag{29}$$

and the volume flow rate is

$$\frac{q}{2} = M\left[\frac{1}{3}h^3 - \frac{1}{\alpha+2}\left|\frac{M}{\tau_0}\right|^{\alpha-1}h^{\alpha+2}\right] - h \tag{30}$$

3.2. Newtonian Case. For the case of a Newtonian fluid (that is $\tau_0 \to \infty$) in an asymmetric channel with no inclination, equations (22) and (26) reduced as follows and are the same as Mishra and Rao [13].

$$u(x,y) = \frac{M}{2}\left[\left(h_1 - \Lambda\right)^2 - \left(y - \Lambda\right)^2\right] - 1 \tag{31}$$

$$q = \frac{M}{6}\left(h_1 - h_2\right)^3 - \left(h_1 - h_2\right) \tag{32}$$

In the case of a Newtonian fluid and a symmetric channel, that is as $\tau_0 \to \infty$ and $\Lambda = 0$ in the absence of inclination, the results are exactly the same as Shapiro *et al.* [21] and reduced as follows:

$$u(x,y) = \frac{M}{2}\left(h^2 - y^2\right) - 1 \tag{33}$$

$$v(x,y) = -Mhh'y + \frac{M'}{2}\left[\frac{y^3}{3} - h_1^2 y\right] \tag{34}$$

$$\psi(x,y) = \frac{M}{2}\left(h^2 y - \frac{y^3}{3}\right) - y \tag{35}$$

$$\frac{q}{2} = M\frac{h^3}{3} - h \tag{36}$$

4. Result and Discussion

In this section, we have analyzed the effects of various fluid parameters, wall parameters, and the angle of inclination that occurred in the model on velocity, pressure pumping, and trapping phenomena. Here the channel parameter $F = (\mu_0 c)/(\rho g d_1^2)$ is dependent on the speed of the peristaltic waves, the viscosity of the fluid, the density of the fluid and the diameter of the channel. This quantity, therefore, varies with changes in the fluid viscosity μ_0, density ρ, wave speed c and the channel width $d_1 + d_2$. The values of F that are used in this study were calculated for appropriate values of μ_0, ρ, c and d_1. The fluid parameters α and τ_0 were chosen based on values obtained experimentally by Kheyfets and Kieweg [7]. The angles of inclination are taken in the range $\theta \in [0, \pi/2]$ and the phase angle ϕ is chosen in the range $[0, \pi]$, here $\theta = 0$, implies no inclination of the channel and choosing $\theta = \pi/2$ means the channel is vertical. Additionally, choosing $\phi = 0$ implies that the upper and lower waves are in phase while $\phi = \pi$ means the waves are totally out of phase. Also, $a = b \neq 0$ and $\phi = 0$ provide the symmetric case which reduces our results to the results of Ali *et al.* [2]. For $a = b = 0$ then we have the simple case of Poiseuille flow. For the fluid parameter $\tau_0 \to \infty$ we have the Newtonian results for which our results confirm the results obtained by Mishra and Rao [13] for zero inclination. Taking $\left|(II_\tau)/(2\tau_0)\right|^{((\alpha-1)/2)} >> 1$ implies that the Ellis fluid model reduces to a Power-law fluid. Hence our results can be compared with the results of Rao and Mishra [19].

4.1. Pumping Performance. From equation (26), we have

$$M\left[\frac{2}{3}\left(h_1 - \Lambda\right)^2\left(2h_1 + h_2\right) - 2\Lambda\left(h_1 - \Lambda\right)^2 + \frac{2}{\alpha+2}\left|\frac{M}{\tau_0}\right|^{\alpha-1}\left(h_1 - \Lambda\right)^{\alpha+2}\right]$$

$$-2\left(h_1 - \Lambda\right) - q = 0 \quad (37)$$

We use this equation to solve for P, using Newton's method. We define

$$L(P) = M\left[\frac{2}{3}\left(h_1 - \Lambda\right)^2\left(2h_1 + h_2\right) - 2\Lambda\left(h_1 - \Lambda\right)^2 + \frac{2}{\alpha+2}\left|\frac{M}{\tau_0}\right|^{\alpha-1}\left(h_1 - \Lambda\right)^{\alpha+2}\right]$$

$$- 2\left(h_1 - \Lambda\right) - q \quad (38)$$

and hence

$$L'(P) = \frac{2}{3}\left(h_1 - \Lambda\right)^2\left(2h_1 + h_2\right) - 2\Lambda\left(h_1 - \Lambda\right)^2 + \frac{2}{\alpha+2}\left|\frac{M}{\tau_0}\right|^{\alpha-1}\left(h_1 - \Lambda\right)^{\alpha+2} \quad (39)$$

Therefore, we determine the value of P using the iteration

$$P_{i+1} = P_i - \frac{L(P_i)}{L'(P_i)} \quad (40)$$

where the initial approximation value is taken as the Newtonian case from Shapiro *et al.* [21], which is

$$P_0 = \frac{q + 2\left(h_1 - \Lambda\right)}{\frac{2}{3}\left(h_1 - \Lambda\right)^3} \quad (41)$$

The pressure rise per unit wavelength is given by the integral

$$\nabla p = \int_0^1 -P dx \quad (42)$$

The variation of pressure rise per unit wavelength ∇p with volume flow rate q for the variation of different parameters is shown in the Figs. 2-6. The effects of the volume flow as well as the fluid parameters α and τ_0 on the pumping performance were observed from Figs. 2(a-b).

In Fig. 2a, $\alpha = 4$ and $\tau_0 = 2, 4$ and $\tau_0 \to \infty$ were considered and it was seen that as τ_0 increases the relationship between ∇p and q rotates clockwise and converges to the Newtonian relation which is linear. $\tau_0 = 2$ and $\alpha = 4, 6$ and 8 were considered in Fig. 2b and it was observed that with an increase in α the curve diverges from the Newtonian result as the fluid displays more non-Newtonian features. In general, both plots showed that as the volume flow rate $q \in \left[-4, 4\right]$ increases the response in ∇p is a reduction. We observed the variation of ∇p with q in Figs. 3(a-b) for different values of θ and ϕ an observed the same general reduction in ∇p with increase in q.
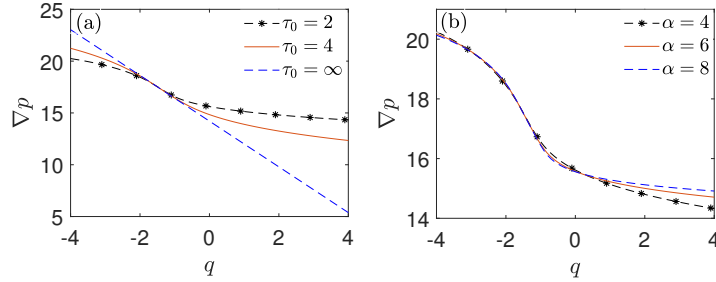
FIGURE 2. ∇p against q for $a = 0.5$ $b = 0.3$ $d = 1.0$ $\phi = \frac{\pi}{3}$ $F = 0.028$ and $\theta = \frac{\pi}{6}$ when   **(a)** $\alpha = 4$ **(b)** $\tau_0 = 2$
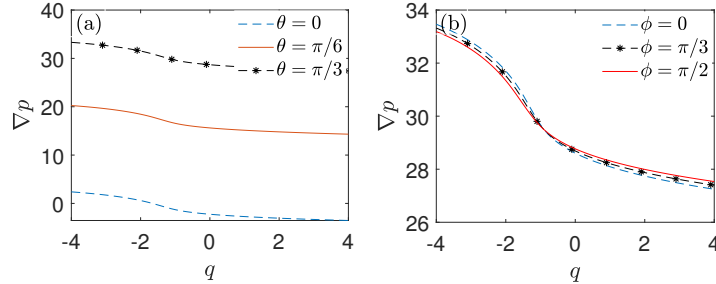

FIGURE 3. ∇p against q for $a = 0.5$ $b = 0.3$ $d = 1.0$ $\alpha = 4$ $\tau_0 = 2$ and $F = 0.028$ **(a)** $\phi = \frac{\pi}{3}$ **(b)** $\theta = \frac{\pi}{3}$

Fig. 3 (a) allowed us to observe the response of the pumping performance to changes in the channel inclination and is plotted for $\phi = \pi/3$ with $\theta = 0, \pi/6$ and $\pi/3$. Fig. 3 (b) on the other hand was generated for $\theta = \pi/3$ with $\phi = 0, \pi/3$ and $\frac{\pi}{2}$, which allows for the analysis of the effects of the phase angle on the pumping performance. Increasing the angle of inclination of the channel results in a uniform increase in the curve of ∇p over q. This means that the pressure rise per unit wavelength required to pump a particular volume flow increases with an increase in θ. Also, with an increase in ϕ the curve of ∇p against q responds by rotating anticlockwise about a point for a critical value of q, at which changes in ϕ has no effect on the curve. Fig. 4 provides a plot of the pressure rise per unit wavelength for the fluid parameter α.

Fig. 4(a) is a plot of ∇p for $b = 0.2, 0.4$ and 0.6 with $d = 1.3$ and Fig. 4 (b) is a plot of ∇p for $b = 0.2$ with $d = 0.5, 0.8$ and 1.3. From these figures, it is observed that for the chosen channel conditions, a monotonic decrease in ∇p with an increase in α. However, for sufficiently small d, ∇p decreases initially and then increases with increase in α and reducing d enough implies that ∇p increases monotonically. Also an increase in b results in an overall decrease in ∇p over α. On the other hand, an increase in d results in a general increase in ∇p against α. Also increasing d in effect increases the channel opening, which means that the pressure required will increase
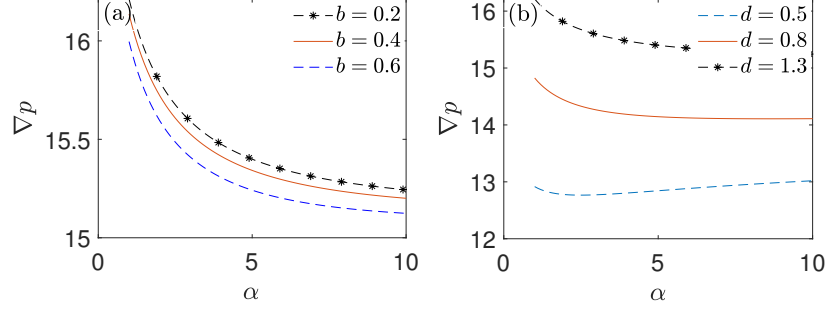
FIGURE 4. ∇p against α for $a = 0.4 \quad \phi = \frac{\pi}{2} \quad \tau_0 = 3.0 \quad F = 0.028 \quad \theta = \frac{\pi}{6}$ and $q = 0.8$ for   **(a)** $d = 1.3$ **(b)** $b = 0.2$
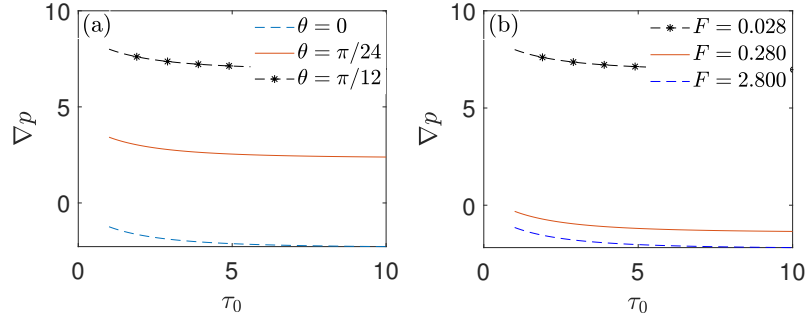
FIGURE 5. ∇p against τ_0 for $a = 0.2 \quad b = 0.2 \quad d = 1.0 \quad \phi = 0 \quad \alpha = 3$ and $q = -0.5$ for   **(a)** $F = 0.028$ **(b)** $\theta = \frac{\pi}{12}$

to compensate for the increase in the channel width. For a fixed volume flow rate increasing b implies a reduction in the channel opening. This implies that the pressure required to compensate for this change to pump at this fixed volume flow rate will reduce. To further analyse the effects of the fluid parameter τ_0, the variation of ∇p against τ_0 is projected in Fig. 5.

Fig. 5a provides a plot of ∇p against τ_0 for $\theta = 0, \frac{\pi}{24}$ and $\pi/12$ with $F = 0.028$. It is seen that an increase in the inclination results in an increase in the pressure rise required to maintain a fixed volume flow rate. Fig. 5b provides a similar relation as in Fig. 5a ($\theta = \frac{\pi}{12}$ and $F = 0.028, 0.280$ and 2.800). In both these plots, we observed that ∇p decreases with increase in τ_0. At about $\tau_0 = 8$, for $\alpha = 3$ we saw that this decrease is minimal and can consider this the limiting case $\tau_0 \to \infty$. Hence , for $\alpha = 3$, we can consider $\tau_0 = 8$ as the limiting case $\tau_0 \to \infty$. Figs. 6(a-b) provide the plots of pressure rise per unit wavelength over the parameter F for different values of q and θ.
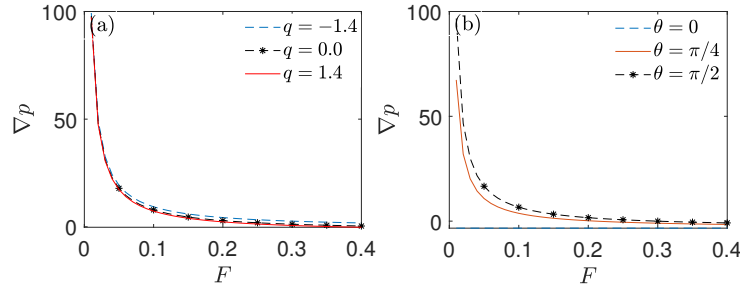
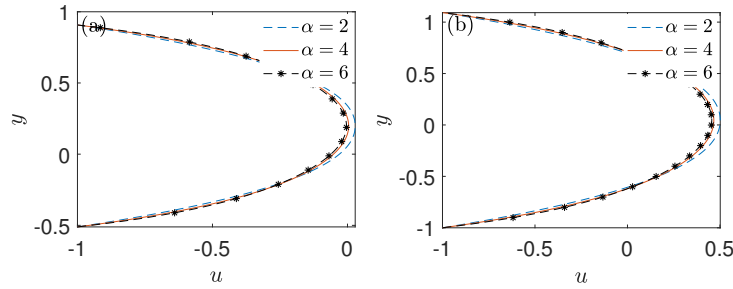FIGURE 6. ∇p against F for $a = 0.7 \quad b = 0.3 \quad d = 1.0$ and $\alpha = 4$ **(a)** $\theta = \frac{\pi}{2}$ **(b)** $q = 0$.

FIGURE 7. u against y for $a = 0.3 \quad d = 1.0 \quad \phi = \frac{\pi}{3}$ and $\tau_0 = 2.0$ **(a)** $b = 0.5 \quad x = 1.3 \quad q = 1.3$ **(b)** $b = 0 \quad x = 0.8$ $q = 0.1$

Fig. 6a is plotted for $\phi = 3\pi/4, \tau_0 = 2$ and $\theta = \pi/2$ for several values of the volume flow rate and the values taken in Fig. 6b are $\phi = \pi/4$, $\tau_0 \to \infty$ and $q = 0$ for $\theta = 0, \pi/4$ and $\pi/2$. We observed that the response in ∇p with an increase in q is a reduction in the value of ∇p over F. From Fig. 6b, we saw that increasing the angle of inclination of the channel implies an increase in ∇p to pump at this fixed volume flow rate. From both these curves, with the chosen parameters a reduction in ∇p with an increase in F was observed. However, for $\theta = 0$ the parameter F has no effect on ∇p.

4.2. Velocity Distribution. The variation of axial velocity u with vertical distance y for different variations of fluid and channel parameters are analysed using the Figs. 7- 9.

Fig. 7a was plotted for $b = 0.5$, at the position $x = 1.3$ and with $q = 1.3$ and Fig. 7b was generated with $b = 0$, at the position $x = 0.8$, for $q = 0.1$ and aimed to analyse the effects of both the fluid parameter α, as well as the volume flow rate, on the velocity. We saw that an increase in the volume flow increases the axial velocity and the velocity of the fluid changes at different sections of the channel. Also, an increase in the fluid parameter α result in a decrease in the axial velocity at the centre of the channel and an increase near the walls of the channel. Due to the Ellis constitutive relation, as the
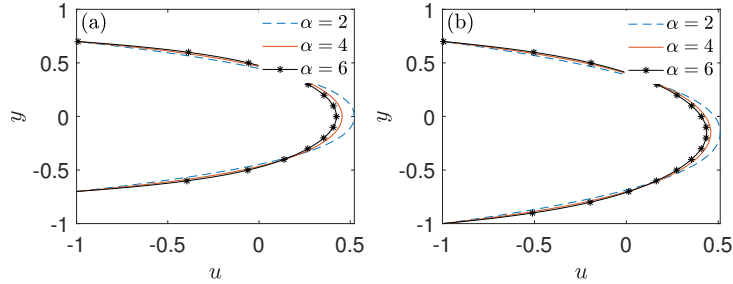
FIGURE 8. u against y at $x = 0.5$ for $a = 0.3$ $b = 0.3$ $d = 1.0$ $\tau_0 = 2.0$ and $q = 0.1$ **(a)** $\phi = 0$ **(b)** $\phi = \frac{\pi}{2}$
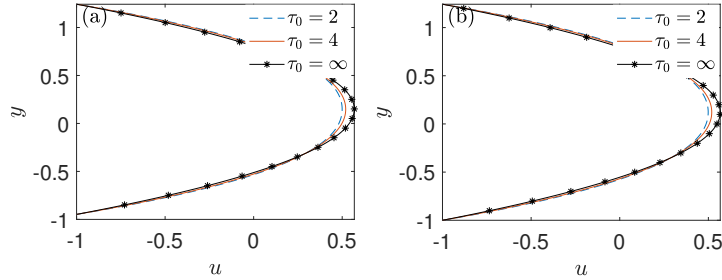

FIGURE 9. u against y at $x = 0.1$ for $a = 0.3$ $d = 1.0$ $\phi = \frac{\pi}{3}$ $\alpha = 2.0$ and $q = 0.1$ **(a)** $b = 0.5$ **(b)** $b = 0$

shear stress increases the effective viscosity of the fluid decreases. Hence, at the centre of the channel the fluid is more viscous than the fluid closer to the walls of the channel. Increasing α would amplify this response in the velocity, which is due to variations in the shear stress and hence the fluid viscosity across the channel width. Again we observe the same response in the axial velocity with the fluid parameter α in Fig. 8. Furthermore, the effect of the phase angle was also determined from these plots.

Fig. 8(a) was produced with $\phi = 0$, while Fig. 8(b) with $\phi = \pi/2$. Changing the phase angle may result in a variation in the width of the channel. Hence, the velocity profiles produced in Fig. 8 at the same section in the channel $x = 0.5$, demonstrates the effects of a widened channel due to changes in the phase angle on the axial velocity. Here the maximum velocity decreased and the rage of the parabolic profile was increased. From Fig. 9 the effects of a change in the fluid parameter τ_0 on the axial velocity was isolated.

Fig. 9a was produced with $b = 0.5$ while Fig. 9(b) with $b = 0$. Increasing τ_0 increases the velocity at the centre of the channel while simultaneously reduces the velocity close to the wall of the channel. The velocity at the wall however was fixed and is given by the no-slip boundary condition. Due to the constitutive relation, we see that an increase in τ_0 increases the effective viscosity of the fluid. Hence, the viscosity of the fluid near the wall of the channel would decrease with an increase in τ_0, since
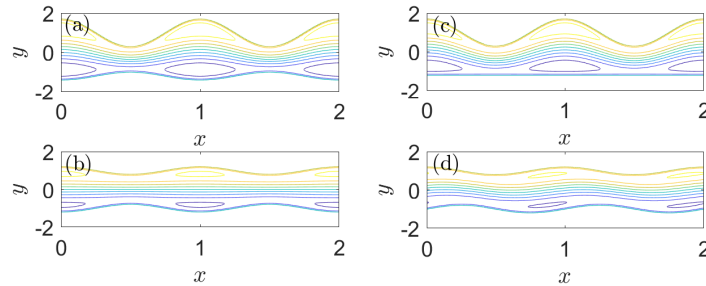
FIGURE 10. ψ for $\alpha = 2.0$ $\tau_0 = 2.0$ $F = 0.028$ $\theta = \frac{\pi}{6}$
and $q = 0.5$ **(a)** $a = 0.7$ $b = 0.2$ $d = 1.2$ $\phi = 0$
(b) $a = 0.2$ $b = 0.2$ $d = 1.0$ $\phi = 0$ **(c)** $a = 0.7$ $b = 0$ $d = 1.2$ $\phi = 0$ **(d)** $a = 0.2$ $b = 0.2$ $d = 1.0$ $\phi = \frac{\pi}{2}$

the shearing forces are greatest in this region. However, as we observed the fluid near the centre of the channel, where least shearing forces are present, the effective viscosity decreases with an increase in τ_0, and hence an increase in the axial velocity is seen at this point. This is a similar but inverted result to the response of the axial velocity to changes in α.

4.3. Streamlines and Trapping. The trapping phenomenon in peristaltic transport was first studied by Shapiro *et al.* [21] for Newtonian fluid flow which describes the development and downstream transport of fluid boluses. Understanding this phenomenon is very important in the physiological system and the theoretical observation made from this can be used to understand the formation of thrombus in the blood. We plotted the streamlines in the wave frame of reference for different parameters of the problem and aimed to analyse the formation of trapped fluid bolus and the plots are projected through Figs. 10-15.

In Fig. 10a and 10c we have taken, $b = 0.2, 0$ respectively $a = 0.7, d = 1.2$, and $\phi = 0$ aimed to notice the effect that the amplitude of the wall has on the streamlines. In Figs. 10b and 10d, we considered $\phi = 0$ and $\pi/2$ respectively when $a = 0.2, b = 0.2, d = 1.0$ and hence we can analyse the effects of the phase angle on the streamlines pattern. In all these plots we saw the formation of the circulations of fluid that moves with the speed of the wave. A reduction of the lower wall amplitude affects the streamlines at the lower wall more significantly and minimally disturbs the upper streamlines. Increasing the phase angle results in a reduction of the circulation of fluid observed in these streamlines. Hence, at $\phi = 0$ the largest circulations are observed and as ϕ increases the size of the bolus decreases and at $\phi = \pi$ there are no circulations present observed for the other parameters fixed as given. Fig. 11a was plotted for $a = 0.6, \phi = \pi/2, \alpha = 2$ and $\tau_0 = 2$ and Figs. 11(b-c) are plotted for $a = 0.2, \phi = 0, \alpha = 4, 2$ and 2 and $\tau_0 = 2, 2$ and 4 in that order. From these plots it is realized that as in the case of changing the lower wall amplitude, changes in the upper wall amplitude affects the upper streamlines and has less influence on the lower streamlines, that is, a change in the upper wall amplitude has more effect on the streamlines near the upper wall and visa versa. Fig. 11(b-d) provide the symmetric case while Fig.11d being the Newtonian case which is
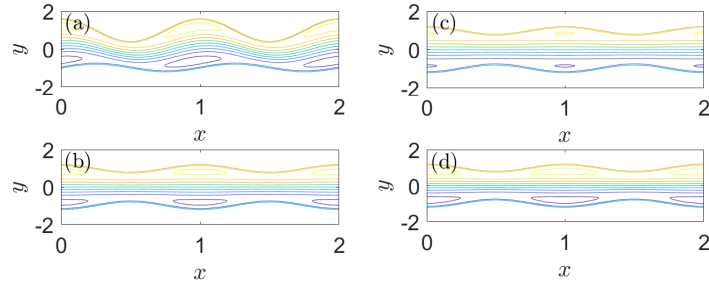
FIGURE 11. ψ for $b = 0.2$ $\quad$ $d = 1.0$ $\quad$ $F = 0.028$ $\quad$ $\theta = \frac{\pi}{6}$ and $q = 0.5$. $\quad$ **(a)** $a = 0.6$ $\quad$ $\phi = \frac{\pi}{2}$ $\quad$ $\alpha = 2$ $\quad$ $\tau_0 = 2$ $\quad$ **(b)** $a = 0.2$ $\quad$ $\phi = 0$ $\quad$ $\alpha = 4$ $\quad$ $\tau_0 = 2$ $\quad$ **(c)** $a = 0.2$ $\quad$ $\phi = 0$ $\quad$ $\alpha = 2$ $\quad$ $\tau_0 = 2$ $\quad$ **(d)** $a = 0.2$ $\quad$ $\phi = 0$ $\quad$ $\alpha = 4$ $\quad$ $\tau_0 = 4$
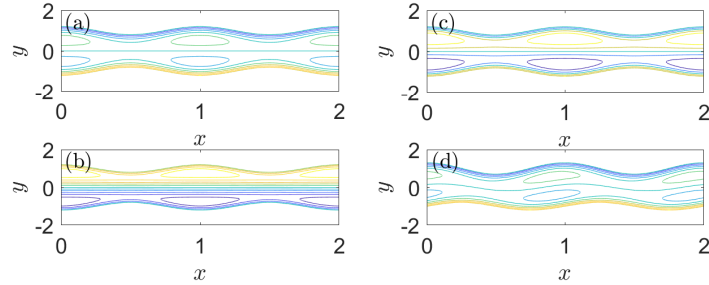
FIGURE 12. ψ for $b = 0.2$ $\quad$ $d = 1.0$ $\quad$ $\alpha = 2.0$ $\quad$ $\tau_0 = 2.0$ $\quad$ $F = 0.028$ and $\theta = \frac{\pi}{6}$. $\quad$ **(a)** $a = 0.2$ $\quad$ $\phi = 0$ $\quad$ $q = -0.4$ $\quad$ **(b)** $a = 0.2$ $\quad$ $\phi = 0, q = -0.2$ $\quad$ **(c)** $a = 0.2$ $\quad$ $\phi = 0$ $\quad$ $q = 0.2$ $\quad$ **(d)** $a = 0.3$ $\quad$ $\phi = \frac{\pi}{2}$ $\quad$ $q = -0.4$

obtained be setting τ_0 large ($\tau_0 > 6$). We also observed that an increase in τ_0 (shifting towards Newtonian nature of the fluid) increases the size of the circulations seen in the streamlines. However, an increase in α has the opposite effect and the fluid will display more non-Newtonian responses with increase in α.

Figs.12 (a-d) provide the streamlines for $a = 0.2, 0.2, 0.2$ and 0.3, $\phi = 0, 0, 0$ and $\pi/2$ and $q = -0.4, -0.2, 0.2$ and -0.4 correspondingly. Here we observed that an increase in the volume flow separates the circulations of fluid in both the symmetric and asymmetric cases. A further increase of the volume flow results in further separation of the circulations mentioned which in turn reduces in size and then diminishes. Also, decreasing the volume flow enough would result in a merging of these circulations at the centre of the channel resulting in the trapping phenomenon. Further reductions in the volume flow would result in a decrease in the trapped region in the centre.

Figs. 13(a-d) demonstrate the transitions of the trapping phenomenon observed in the streamlines. The streamlines are plotted for $q = -0.85, -0.7, -0.6$ and -0.45
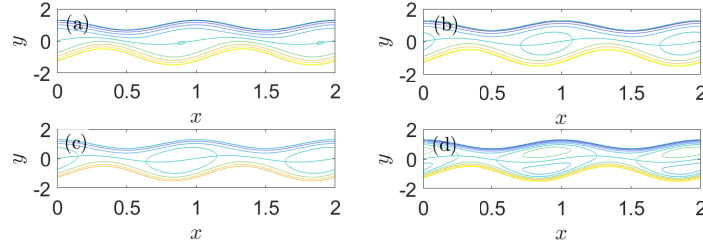
FIGURE 13. ψ for $a = 0.3$ $b = 0.5$ $d = 1.0$ $\phi = \frac{\pi}{3}$ $\alpha = 4.0$ $\tau_0 = 2.0$ $F = 0.028$ and $\theta = \frac{\pi}{6}$. **(a)**$q = -0.85$ **(b)** $q = -0.7$ **(c)** $q = -0.6$ **(d)** $q = -0.45$
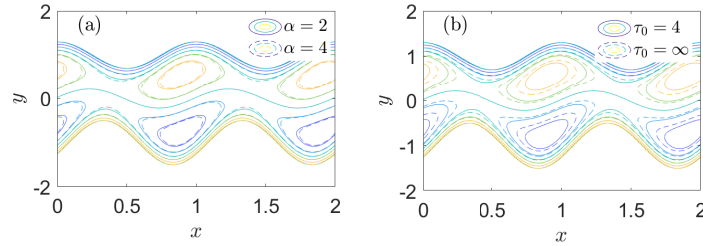

FIGURE 14. ψ for $a = 0.3$ $b = 0.5$ $d = 1.0$ $\phi = \frac{\pi}{3}$ $F = 0.028$ $\theta = \frac{\pi}{6}$ and $q = -0.3$ **(a)** $\tau_0 = 2$ **(b)** $\alpha = 4$

respectively. Here we highlight the effect of changes in the volume flow rate on the trapped region. Fig. 13(a) and (d) provides images of the limiting cases of trapping. From Fig. 13a, any further reduction in the volume flow rate will result in a reduction in the trapped region until the region no longer exists. On the other hand, from Fig. 13d we have observed the other extreme. Any further increase in the volume flow rate implies a splitting of the trapped region which suggests that this trapped region would no longer exist. Increase in the volume flow rate in this region serves to increase the size of the trapped region.

In Fig. 14a the streamlines are plotted with $\alpha = 2$ and 4 and $\tau_0 = 2$, while Fig. 14b gives the streamlines with $\alpha = 4$ and $\tau_0 = 2$ and $\tau_0 \to \infty$. Here we isolated and observed the effects of the fluid parameters α and τ_0 on the streamlines. We observed a reduction in the size of the circulations present in the streamlines with increase in the fluid parameter α, and an increase with increase in the parameter τ_0. Increasing α results in the fluid displaying greater non-Newtonian characteristics while increasing τ_0 implies that the fluid characteristics converges to Newtonian.

Using the streamlines and the velocity vectors along with the stream line values, Fig. 15 provides more insight in the reflux and trapping occurrence. Fig.15a was generated with $a = b = 0.3, \phi = 0$ and $\tau_0 \to \infty$. This provides the Newtonian result within a symmetric channel. Fig. 15b on the other hand, was generated with $a = 0.4, b = 0.3, \phi = \pi/3$ and $\tau_0 = 2$. We observe in both Figs.15a and 15b reflux
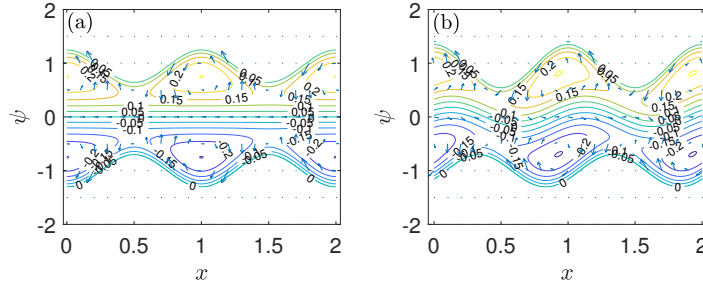
FIGURE 15. ψ for $d = 1.0$ $\quad F = 0.028$ $\quad \theta = \frac{\pi}{6}$ and $\quad q = 0$ $\quad$ **(a)** $a = b = 0.3$ $\quad \phi = 0$ $\quad \tau_0 \to \infty$ $\quad$ **(b)** $a = 0.4$ $\quad b = 0.3$ $\quad \phi = \frac{\pi}{3}$ $\quad \tau_0 = 2$

at the walls by observing the difference of the streamline values at the walls, which indicate a negative volume flow rate. It is also seen from the velocity vectors that the fluid in the trapped region circulates as it moves forward with the wave.

5. Conclusions

Based on the observations made, the following are the conclusions that can be made:

- The fluid parameters α and τ_0 have a greater effect on ∇p than on the stream-lines pattern and the axial velocity. Now, any changes in either parameter that deviate from the Newtonian case results in a reduction of the circulations observed in the streamlines an increase in u near the walls of the channel, a simultaneous reduction in u at the centre of the channel and anticlockwise rotation of the curve of ∇p against q about a critical value of q.
- The channel parameters (that is, the channel width d, wall amplitude a, b and phase angle ϕ) have relatively greater effects on the flow. Now, increasing d results in an increase in the size of the circulations of fluid observed in the streamlines and increases ∇p for a fixed value of q. An increase in the amplitude of the wave also increases the size of the observed circulations but reduces ∇p. Increasing ϕ on the other hand results in a reduction of the size of the circulations in the streamlines and an anticlockwise rotation of the plot ∇p over q from the symmetric case about a critical value of q.
- The angle of inclination of the channel θ, has no effect on the axial velocity u and hence the streamlines within the channel, since the volume flow rate was fixed. However, the inclination has a direct relation with the pressure rise per unit wavelength ∇p. That is, an increase θ implies a responsive increase in the ∇p for a fixed value of q.
- The effect of the dimensionless parameter F, is the same as the effects that θ has on the flow.
- For a fixed channel width, amplitude and phase angle, the stages of trapping is observed with increase in q from the streamlines, and trapping is confirmed to exists within a range of values of q.

Conflicts of interest : The authors declare no conflict of interest.

Data availability : Not applicable

References

1. F.M. Abbasi, T. Hayat, B. Ahmad, and G.Q. Chen, *Peristaltic Motion of a non-Newtonian Nanofluid in an Asymmetric Channel*, Zeitschrift fur Naturforschung a **69** (2014), 451-461.

2. N. Ali, A. Abbasi and I. Ahmad, *Channel flow of Ellis fluid due to peristalsis*, American Institute of Physics (AIP) Advances **5** (2015), 097214(1)-(9).

3. N.T.M. Eldabe, O.M. Abo-Seida, A.A.S. Abo-Seliem, A.A. ElShekhipy and N. Hegazy, *Peristaltic Transport of Magnetohydrodynamic Carreau Nanofluid with Heat and Mass Transfer inside Asymmetric Channel*, American Journal of Computational Mathematics **7** (2017), 1-20.

4. M.E. Gendy, O.A. Bég, A. Kadir, M.N. Islam and D. Tripathi, *Computational fluid dynamics simulation and visualization of Newtonian and non-Newtonian transport in a peristaltic micro-pump*, Journal of Mechanics in Medicine and Biology **21** (2021), 2150059.

5. Y.C. Fung and C.S Yih, *Peristaltic transport*, Journal of Applied Mechanics **35** (1968), 669-675.

6. T. Hayat, Y. Wang, A.M. Siddiqui, K. Hutter and S. Asghar, *Peristaltic transport of a third-order fluid in a cicular cylindrical tube*, Mathematical Models and Methods in Applied Sciences **12** (2002), 1691-1702.

7. V.O. Kheyfets and S.L. Kieweg, *Gravity-Driven Thin Film Flow of an Ellis Fluid*, Journal of Nonnewtonian Fluid Mechanics **202** (2013), 88-98.

8. M. Kothandapani and S. Srinivas, *Non-linear peristaltic transport of a Newtonian fluid in an inclined asymmetric channel through a porous medium*, Physics Letters A **372** (2008), 1265-1276.

9. P. Hariharan, V. Seshadri and R.K. Banerjee, *Peristaltic transport of non-Newtonian Fluid in a diverging tube with different wave forms*, Mathematical and Computer Modelling **48** (2008), 998-1017.

10. T.W. Latham, *Fluid motions in a peristaltic pump*, Cambridge, MA, Massachusetts, 1966.

11. M.J. Manton, *Long-wavelength perestaltic pumping at low Reynolds number*, Journal of Fluid Mechanics **68** (1975), 467-76.

12. A. Mernone, J. Mazumdar and S.K. Lucas, *A mathematical study of peristaltic transport of a casson fluid*, Mathematical and Computer Modelling **35** (2002), 895-912.

13. M. Mishra, A.R. Rao, *Peristaltic transport of a Newtonian fluid in an asymmetric channel*, Z. angew. Math. Phys. **54** (2003), 532–550.

14. S. Nadeem, S. Akhtar and A. Saleem, *Peristaltic flow of a heated Jeffrey fluid inside an elliptic duct: streamline analysis*, Appl. Math. Mech.-Engl. Ed. **42** (2021), 583–592.

15. P. Naga Rani and G. Sarojamma, *Peristaltic transport of a Casson fluid in an asymmetric channel*, Australas Phys. Eng. Sci. Med. **27** (2004), 49-59.

16. P. Nagarani and A. Lewis, *Peristaltic flow of a Casson fluid in an annulus*, Korea-Australia Rheology Journal **24** (2012), 1-9.

17. Q.H. Nguyen and H.D. Nguyen, *Incompressible Non-Newtonian Fluid Flows*, Continuum Mechanics-Progress in Fundamentals and Engineering Applications **1** (2012), 47-72.

18. S. Noreen, T. Kausar, D. Tripathi, Qurat Ul Ain and D.C. Lu, *Heat transfer analysis on creeping flow Carreau fluid driven by peristaltic pumping in an inclined asymmetric channel*, Thermal Science and Engineering Progress **17** (2020), 100486.

19. A.R. Rao and M. Mishra, *Peristaltic transport of a power-law fluid in a porous tube*, Journal of Non-newtonian Fluid Mechanics **121** (2004), 163-174.

20. S. Saleem, S. Akhtar, S. Nadeem, A. Saleem, M. Ghalambaz and A. Issakhov, *Mathematical study of Electroosmotically driven peristaltic flow of Casson fluid inside a tube having*

systematically contracting and relaxing sinusoidal heated walls, Chinese Journal of Physics **71** (2021), 300-311.

21. A.H. Shapiro, M.Y. Jaffrin, S.L, Weinberg, *Peristaltic pumping with long wavelengths at low Reynolds number*, Journal of Fluid Mechanics **1** (1969), 799-825.

22. L.M. Srivastava and V.P. Srivastava, *Peristaltic Transport of a Non-Newtonian Fluid: Application to the Vas Differens and Small Intestine*, Annals of Biomedical Engineering **13** (1985), 137-153.

23. S. Srinivas and R. Gayathri, *Peristaltic transport of a Newtonian fluid in a vertical asymmetric channel with heat transfer and porous medium*, Applied Mathematics and Computation **215** (2009), 185-196.

24. R.T. Steller, *Generalized slit flow of an Ellis fluid*, Polymer Engineering and Science **41** (2001), 1859-1870.

25. S. Usha and A.R. Rao, *Peristaltic transport of two-layered power-law fluids*, Journal of Biomechanical Engineering-transactions of The Asme **119** (1997), 483-488.

26. K. Vajravelu, S. Sreenadh and V.R. Babu, *Peristaltic pumping of a Herschel–Bulkley fluid in a channel*, Applied Mathematics and Computation **169** (2005), 726-735.

27. K.K. Vajravelu, S. Sreenadh and V.R. Babu, *Peristaltic pumping of a Herschel-Bulkley fluid in a channel*, International Journal of Non-linear Mechanics **40** (2005), 83-90.

A. Small received a M.Phil from the University of the West Indies, Mona Campus, Jamaica and is presently persuing a Ph.D. from the same. Presently he is working at the Caribbean Maritime Univeristy, Jamaica as a Senior Lecturer. His research interests include fluid mechanics and numerical methods.

Department of Mathematics, The University of the West Indies, Mona Campus, Kingston 7, Jamaica West Indies.
Faculty of Engineering, Caribbean Maritime University, Norman Manley Highway, Palisadoes Park, Kingston, Jamaica West Indies.
e-mail: kirbysmall@hotmail.com

P. Nagarani received a M.Sc., M.Phil and Ph.D. from Sri Padmavati Women's University, Andra Pradesh, India. She is currently a Senior Lecturer at the University of the West Indies, Mona Campus, Jamaica, West Indies. Her research interests are Physiological Fluid Dynamics and Advanced Mathematical Methods.

Department of Mathematics, The University of the West Indies, Mona Campus, Kingston 7, Jamaica West Indies.
e-mail: nagarani_ponakala@yahoo.co.in

M. Narahari received a Ph.D. from Sri Venkateswara University, Andra Pradesh, India. He is currently a Lecturer at Universiti Teknologi PETRONAS, Malaysia. His reasearch interests are Computational Fluid Dynamaics, Convective heat tranfer and Non-Newtonian fluid flow.

Fundamental and Applied Sciences Department, Universiti Teknologi PETRONAS, 32610 Seri Iskandar, Perak Darul Ridzuan, Malaysia.
e-mail: naraharim6@gmail.com